Applied Catalysis B: Environmental 163 (2015) 323–329

Contents lists available at ScienceDirect

Applied Catalysis B: Environmental

journal homepage: www.elsevier.com/locate/apcatb

Morphological effect on photocatalytic degradation of Rhodamine B and conversion of active species over $BaSb_2O_6$

Jing Chen, Danzhen Li*, JuBao Wang, Peng Wang, Changsheng Cao, Yu Shao, Jinxiu Wang, Jiangjun Xian

Research Institute of Photocatalysis, State Key Laboratory of Photocatalysis on Energy and Environment, Fuzhou University, Fuzhou 350002, PR China

ARTICLE INFO

Article history:
Received 1 June 2014
Received in revised form 29 July 2014
Accepted 9 August 2014
Available online 19 August 2014

Keywords:
Antimonate
Photocatalysis
Morphology
Mechanism

ABSTRACT

Both active species and morphological effect are important for antimonate photocatalysis. However, there is little research on the relationship between them. The aims of this article are to investigate the relationship between morphological effect and mutual transformation of active species during photocatalytic degradation of Rhodamine B (RhB) over $BaSb_2O_6$. The existence of active species is confirmed by electron spin-resonance spectroscopy (ESR), photoluminescence method and N,N-diethyl-p-phenylenediamine (DPD) method. The role of active species is evaluated by adding scavengers of active species during the photocatalytic degradation of RhB, and the mutual transformation of active species are investigated by observing the influence of different conditions on H_2O_2 in the photocatalytic processes. The results show that the concentration of $^{\bullet}OH$ has the greatest influence on photocatalytic activity of $BaSb_2O_6$. As the sources of $^{\bullet}OH$, the production of $HO_2^{\bullet}/O_2^{\bullet-}$ and surface hydroxyl groups are dependent on the morphology of the sample. The concentrations of $HO_2^{\bullet}/O_2^{\bullet-}$ and surface hydroxyl groups are higher on marigold-flower-like $BaSb_2O_6$ than that on rose-flower-like $BaSb_2O_6$. The morphological effect of $BaSb_2O_6$ may be applied similarly to other antimonate photocatalysts.

1. Introduction

As a group of stable and efficient photocatalysts, antimonates have attracted a great deal of attention. Up to date, various antimonate photocatalysts have been developed, such as $M_2Sb_2O_7$ (M = Ca, Sr) [1–5], MSb_2O_6 (M = Ca, Sr, Ba) [2,6,7], $CaSb_2O_5(OH)_2$ [8–10], $Cd_2Sb_2O_{6.8}$ [11], $CuSb_2O_6$ [12], $BiSbO_4$ [13,14], $PbSb_2O_6$ [15], $AgSbO_3$ [16–19], $ZnSb_2O_6$ [20,21] and $SnSb_2O_7$ [22]. Some of them have been reported to possess high photocatalytic activity in degradation of benzene and organic dyes, while the others are relatively inactive. Several reasons have been proposed to explain why antimonates show different photocatalytic performances. First, the crystal structures of antimonates influence their photocatalytic performance greatly. Sato et al. proposed that the distorted Sb–O polyhedra in the structures of antimonates might be photocatalytically active [2,23–25]. The magnitude and the direction of lattice distortion are associated with the photocatalytic performance [26]. Lin et al. believed that the crystal packing factor (PF) might also be the reason of the different activities among the antimonates [7,10]. Second, the photocatalytic performances of antimonates are dependent on morphology. For instance, nanocrystalline antimonates prepared by hydrothermal synthesis are proven to have higher quantum yields compared with its bulk phase prepared by solid state synthesis [1] because nanocrystals usually have large specific surface area. Indeed, the morphology of antimonate is related to many properties of antimonate, such as BET specific surface area, pore size distributions, adsorption of pollutants and the light propagation mode, etc [27–32]. All of above are macroscopic physicochemical properties and closely relate to the morphology of antimonate, but they are not the determinant of their photocatalytic activities. Thus, there are still unknown links between these macroscopic properties and the photocatalytic activity. This paper aims to find one of unknown links between the morphology and photocatalytic activities of antimonate. To our knowledge, detailed research on the morphological effect of antimonate is rare.

Photocatalytic reaction is based on the transfer or exchange of photo-generated electrons between the adsorption molecules and photocatalyst. More attention should be paid to the morphological effect on the formation and conversion of active species. During the photocatalytic degradation of organic pollutants over the photocatalyst, active oxygen species with high reactivity are

* Corresponding author. Tel.: +86 591 83779256; fax: +86 591 83779256.
E-mail addresses: dzli@fzu.edu.cn, danzli@126.com (D. Li).

http://dx.doi.org/10.1016/j.apcatb.2014.08.014
0926-3373/

important, such as hydroxyl radicals (•OH), superoxide radicals ($O_2^{\bullet-}$) and H_2O_2. Many papers attribute photocatalytic activities to these active species. However, what role does each species play? Which is the most important active species? What are the sources of these active species? What is the relationship between these active species and the photocatalytic degradation process? Some conceptions have been given by investigating TiO_2 [33,34]. Nevertheless, these results cannot reflect the true condition of antimonates photocatalysis because the Sb–O polyhedra in the structure of antimonates are different from the Ti–O polyhedra in the structure of TiO_2.

To investigate the "real morphological effect" on mutual transformation of active species during antimonate photocatalysis, it is necessary to exclude the influences of crystal structure on the photocatalytic activities, such as crystalline structure, crystallinity and crystal packing factor, etc. In this study, $BaSb_2O_6$ synthesized in our lab is chosen as the object [6] because $BaSb_2O_6$ has identical characteristics (wide band gap and Sb–O polyhedra in crystal cell) with other antimonates. Marigold-flower-like $BaSb_2O_6$ (M-$BaSb_2O_6$) and rose-flower-like $BaSb_2O_6$ (R-$BaSb_2O_6$) are two kinds of $BaSb_2O_6$ with different morphologies. The morphologies, optical properties, crystallinity, surface areas and pore structures of R-$BaSb_2O_6$ and M-$BaSb_2O_6$ are shown in Fig. S1. The reason for choosing the two kinds of $BaSb_2O_6$ is that the morphologies and the photocatalytic activities of them are different, while the crystalline structure, crystallinity and crystal packing factor of them are similar. In this paper, active species such as hydroxyl radicals (•OH), superoxide radicals ($HO_2^{\bullet}/O_2^{\bullet-}$), holes ($h^+$) and hydrogen peroxide (H_2O_2) involved in the photocatalytic degradation process of Rhodamine B are detected by several techniques, then morphological effect on photocatalytic degradation of Rhodamine B and mutual transformation of active species over $BaSb_2O_6$ are discussed in detail.

2. Materials and experiments

2.1. Materials

5, 5-Dimethyl-1-pyrroline-N-oxide (DMPO) was obtained from Sigma Co. Ltd. Tert-butyl alcohol (TBA), benzoquinone (BQ) and ethylenediaminetetraacetic acid (EDTA) were from Sinopharm Chemical Reagent Co., Ltd. Terephthalic acid (TA) is from Acros Chemical Co., and horseradish peroxidase (POD) and N, N-diethyl-p-phenylenediamine (DPD) were from J&K Chemical Ltd. Barium acetate [$Ba(CH_3COO)_2{\cdot}2H_2O$] and Rhodamine B (RhB) were from Tianjing Chemical Reagent Co., Ltd. $K_2Sb_2O_{11}H_{10}$ was from Shanghai Chemical Reagent Co., Ltd., and Catalase was from Shanghai yuanye Bio-Technology Co., Ltd. Deionized water was used in all experiments.

2.2. Preparation of photocatalyst

Marigold-flower-like $BaSb_2O_6$ (M-$BaSb_2O_6$) and rose-flower-like $BaSb_2O_6$ (R-$BaSb_2O_6$) were synthesized according to our previous article [6]. Appropriate amount of $Ba(CH_3COO)_2{\cdot}2H_2O$ was dissolved in 10 mL of deionized water followed by adding 25 mL of 0.1 mol L^{-1} $KSb(OH)_6$ solution. Then the suspension was diluted to 75 mL. Finally, its pH value was adjusted to 3. After being stirred at room temperature for 12 h, the suspension was transferred into a Teflon-lined stainless autoclave and was heated at 200 °C for 5 h. As the autoclave was cooled to room temperature, the white precipitation was obtained at the bottom of autoclave and was collected by centrifugation. The collected precipitation was washed alternately with deionized water, and dried in 80 °C oven.

$$-OH\ (acid) + Na^+ + OH^- \rightarrow -O-Na^+ + H_2O$$

Scheme 1. The reaction between NaOH and acidic hydroxyl groups.

2.3. The quantities of surface hydroxyl groups

The quantities of hydroxyl groups on the surface of metal oxides can be semi-quantitatively analyzed by acid–base titration [35,36]. The reaction mechanism was shown in Scheme 1. According to Ref. [37], the quantity of acidic hydroxyl groups on the surface of oxide is equal to that of base hydroxyl. Therefore, only the quantities of acidic hydroxyl groups over different samples were compared in this paper. The surface acidic hydroxyl groups of $BaSb_2O_6$ were treated by NaOH solution with pH ≈11 to ensure that most of acidic hydroxyl groups can be changed into its conjunction base [35]. The procedure was as follows: $BaSb_2O_6$ powders were dispersed in 50 mL of NaOH solution (2 mmol L^{-1}) at room temperature respectively. After stirring for 12 h, the suspension was separated using centrifuge and the supernate was retrieved, and then the acid–base titration was carried out by 3 mmol L^{-1} HNO_3 to determine the consumption of NaOH caused by reaction between NaOH and the acidic hydroxyl groups on the surface of $BaSb_2O_6$.

2.4. Characterization of photocatalysts

The UV–vis spectra of liquid samples were carried out on Varian Cary 50 UV–Vis spectrophotometer. ESR (electron spin-resonance spectroscopy) spectra were performed on a Bruker model A300 spectrometer with a 254 nm UV light source. The settings were center field, 3512 G; microwave frequency, 9.86 GHz; power, 20 mW. The photoluminescence spectra were obtained by an Edinburgh FL/FS900 spectrophotometer. The generation of •OH radicals was investigated by the method of photoluminescence with terephthalic acid (PL-TA) [38]. X-ray photoelectron spectroscopy (XPS) measurements were conducted on an ESCALAB 250 photoelectron spectroscope (Thermo Fisher Scientific) at 3.0×10^{-10} mbar with Al Ka X-ray beam (1486.6 eV). Acid–base titration was carried out on the ZDJ-4A automatic potentiometric titrimeter (INESA Scientific Instrument Co., Ltd.). The concentration of dissolved oxygen (DO) is monitored by a DO Probe (Thermo Scientific ORION 081010MD, USA).

2.5. Test of photocatalytic activity

UV-light photocatalytic experiments were conducted in a quartz reactor surrounded by four UV lamps (Philips, TUV 4W/G4 T5 and the wavelength centered at 254 nm). A 0.15 g of photocatalyst was added into 150 mL of RhB solution (1×10^{-5} mol L^{-1}). Prior to UV irradiation, the suspensions were magnetically stirred for 20 min to reach the adsorption and desorption equilibrium. After irradiation, 4 mL of the suspensions was sampled at given time intervals, followed by centrifuged to retrieve the supernate. Then the concentrations of supernate were analyzed by a Varian Cary 50 Scan UV-Vis spectrophotometer. Photocatalytic conversion ratio (PCR) is recognized as $1 - C_t/C_0$, where C_0 is the adsorption equilibrium concentration and C_t is the concentration at time t. The temperature was kept at 25 °C during the photocatalytic processes.

3. Results and discussion

3.1. Detection of the active species

3.1.1. Detection of active species by scavengers

It is well established that the photocatalytic degradation of organic pollutants is initiated by reactive species, such as valence

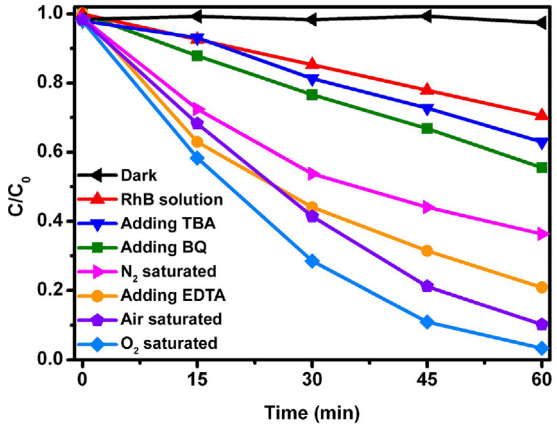

Fig. 1. Adsorption-equilibrium of RhB over M-$BaSb_2O_6$ in dark, photolysis of RhB solution and photocatalytic degradation of RhB over M-$BaSb_2O_6$ in the different conditions exposed to UV light: adding 200 μL of TBA, 2 mg BQ, N_2 saturated, 1×10^{-3} mol L^{-1} EDTA, air saturated and O_2 saturated.

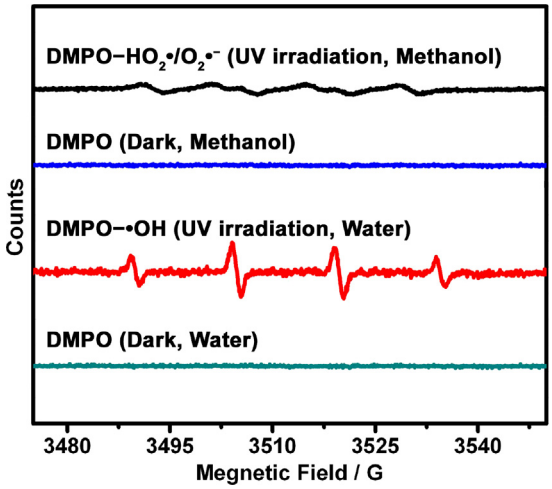

Fig. 2. The DMPO–•OH and the DMPO–HO_2•/O_2•− ESR signal over M-$BaSb_2O_6$.

band holes (h^+), hydroperoxyl radical or superoxide radicals ($HO_2/O_2^{\bullet-}$), hydroxyl radicals (•OH) and hydrogen peroxide (H_2O_2) [39]. The roles of these reactive species are evaluated by investigating the effects of scavengers of active species on photocatalytic degradation of RhB. The aqueous solution of RhB is stable in darkness. After irradiated by UV light for 1 h, 70% of RhB remains, as shown in Fig. 1.

Fig. 1 also illustrates the photocatalytic degradation of RhB over M-$BaSb_2O_6$ in different conditions. The PCR of RhB on M-$BaSb_2O_6$ reaches 90% in absence of scavengers. The greatest influence on the photocatalytic activities of M-$BaSb_2O_6$ is brought by adding 200 μL of TBA that is the scavenger of hydroxyl radical and the PCR of RhB is dramatically reduced to 37%. This indicates that •OH plays the most important role in this reaction. The second greatest influence is brought by BQ, a HO_2•/O_2•− scavenger. After adding 2 mg BQ, the PCR of RhB is reduced to 44.5%. HO_2•/O_2•− can be produced by the combination between Dissolved oxygen (DO) and one electron. To investigate the influence of DO, the photocatalytic reactions are monitored in the O_2 saturated and N_2 saturated conditions. The PCR of RhB is increased by 10% in the O_2 saturated condition, while in the N_2 saturated condition it is decreased by 26%. Fig. S2 shows that the concentration of DO is maintained at 2% in the N_2 saturated condition both in dark and under UV irradiation. The result indicates that the DO is almost diminished in N_2 saturated condition. EDTA, a scavenger of valence band hole, is added into the system to detect the influence of valence band hole on the photocatalysis. The addition of EDTA provokes somewhat inhibition of the RhB degradation and it changes the path of the degradation. As it is shown in Fig. S3, photocatalytic degradation of RhB solution over M-$BaSb_2O_6$ without adding any scavenger is a deethylation process. The maximum value of absorption peak of RhB shows blue shift during the photocatalytic reaction, while the addition of EDTA diminishes the blue shift. This indicates that the deethylation process of RhB is closed related to photogenerated hole.

3.1.2. Detection of reactive oxygen species by ESR

The generation of reactive oxygen species is confirmed by an ESR spin trapping technique with DMPO as a spin-trapping reagent in the UV irradiation condition. From Fig. 2, no ESR signals can be observed in the presence of M-$BaSb_2O_6$ and DMPO either in water or in methanol without irradiation. By UV light irradiation, ESR quartet characteristic of DMPO–•OH and ESR sextet characteristic of DMPO–HO_2•/O_2•− are afforded. Thus, •OH and HO_2•/O_2•− indeed exist in the system.

3.2. Discussion of the photocatalytic mechanism of $BaSb_2O_6$

3.2.1. The positions of the conduction band and valance band of $BaSb_2O_6$

To explain the photocatalytic mechanisms on $BaSb_2O_6$, the positions of the bottom of conduction band and the top of valance band are evaluated. It is assumed that the corresponding conduction and valence band positions of $BaSb_2O_6$ are at the point of zero charge through the following Eqs. (1)–(3) [40,41].

$$\chi_i = \frac{1}{2}(A_f + I_1)^{m_i} \quad (1)$$

$$\chi = \sum_{i=1}^{n} \sqrt[m_i]{\prod_{i=1}^{n}(\chi_i)^{m_i}} \quad (2)$$

$$E_{CB} = \chi - E_0 - \frac{1}{2}E_g \quad (3)$$

where χ_i is the electronegativity of the atom, I_1 and A_f are the first ionization potential and the atomic electron affinity, respectively. χ is the bulk electronegativity of the compound, and m is the oxidation number of the atom; E_g is the band gap energy of the semiconductor, and E_0 is the energy of free electrons on the hydrogen scale (about 4.5 eV) [40,41]. The position of the valence band edge is determined by $E_g = E_{VB} - E_{CB}$. The band gap of $BaSb_2O_6$ is evaluated as ~4.7 eV from the UV–vis spectrum [6]. The calculation result shows that the bottom of the conduction band of $BaSb_2O_6$ is around −0.88 V versus normal hydrogen electrode (NHE) and the top of the valence band is around 3.86 V (vs NHE). Thus, the bottom of conduction band should be higher than the energy level of O_2/HO_2• (−0.13 V vs NHE) and O_2/O_2•− (−0.33 V vs NHE), while the top of valance band should be lower than the •OH/OH^- (2.38 V vs NHE). As shown in Fig. 2, both of the •OH and HO_2•/O_2•− can be detected in the system of $BaSb_2O_6$. In addition, the energy levels of O_2/H_2O_2 (0.68 V vs NHE), HO_2•/H_2O_2 (1.50 V vs NHE) and H_2O/H_2O_2 (1.80 V vs NHE) are also located in the band gap of $BaSb_2O_6$.

3.2.2. Mutual transformation among reactive oxygen species through H_2O_2

Mutual transformations among active species often take place during photocatalysis. Then, we will discuss the role of H_2O_2 and reveal how these active species convert into one another. H_2O_2 is relatively stable and serves as a storage tank of other more reactive oxygen species in the photocatalytic processes. For example, H_2O_2 can be formed by the reduction of O_2, dimerization of •OH

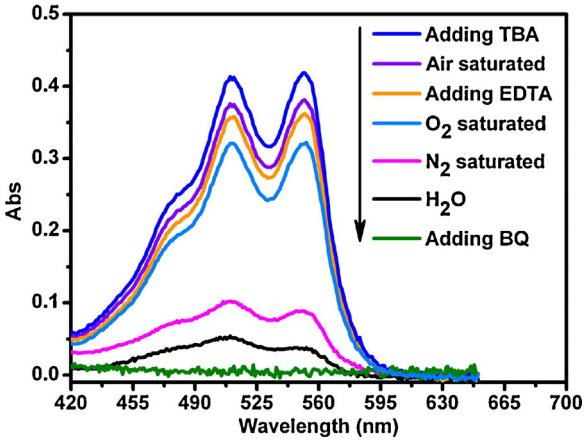

Fig. 3. Detection of H_2O_2. The black curve is obtained by the addition of DPD and POD to water without photocatalyst after 30 min UV irradiation. Other curves (with photocatalyst) are obtained by the same procedure except different conditions are controlled prior to the addition of DPD and POD.

and oxidation of H_2O. Photolysis of H_2O_2 can directly produce •OH, then •OH would attack H_2O_2 to yield HO_2•, while HO_2• also has the ability to react with H_2O_2 to yield •OH. Thus, the more H_2O_2 is detected, the more reactive oxygen species should be formed in the system. The transition among reactive oxygen species in the system through H_2O_2 is shown in reactions (4)–(11).

$$O_2 + e^- \rightarrow O_2^{\bullet -} \quad (4)$$

$$HO_2^{\bullet} \rightleftharpoons O_2^{\bullet -} + H^+ \quad pK_a = 4.8 \quad (5)$$

$$O_2 + 2e^- + 2H^+ \rightarrow H_2O_2 \quad (6)$$

$$2^{\bullet}OH \rightarrow H_2O_2 \quad (7)$$

$$2h^+ + 2H_2O \rightarrow H_2O_2 + 2H^+ \quad (8)$$

$$H_2O_2 \rightarrow 2^{\bullet}OH \quad (9)$$

$$H_2O_2 + {}^{\bullet}OH \rightarrow HO_2^{\bullet} + H_2O \quad (10)$$

$$H_2O_2 + HO_2^{\bullet} \rightarrow {}^{\bullet}OH + O_2 + H_2O \quad (11)$$

The DPD method is employed for the detection of H_2O_2 in this system. This method is based on the horseradish peroxidase (POD)-catalyzed oxidation by H_2O_2 of DPD [42]. As shown in Fig. 3, a weak H_2O_2 signal can be detected by the addition of DPD and POD to water after 30 min UV irradiation. In contrast, the signal is enhanced largely by adding M-$BaSb_2O_6$. Then, the influence of •OH, HO_2•/$O_2^{\bullet -}$, valence band hole and different atmospheres on the H_2O_2 production in this system will be discussed as follow.

The signal of H_2O_2 is almost diminished by adding BQ. Thus, most of the H_2O_2 may be derived from HO_2•/$O_2^{\bullet -}$ which is a key intermediate of the transition from O_2 to H_2O_2. To investigate how much DO participate the process of forming H_2O_2, N_2 is bubbling into the system. In contrast to the situation of adding BQ, the signal of H_2O_2 is reduced largely, but cannot be eliminated. The great difference between air saturated and N_2 saturated condition should come from DO. Hence, DO → HO_2•/$O_2^{\bullet -}$ → H_2O_2 is the main approach to produce H_2O_2 (reactions (4)–(6)). A slightly lower signal strength of H_2O_2 caused by addition of EDTA suggests that the valence band hole is also a source of H_2O_2 (reaction (8))[43]. By UV light irradiation, reactions (7) and (9) usually take place. It is hard to point out which one is in the ascendant. Peculiarly, the H_2O_2 signal strength is increased by adding TBA which is the scavenger of •OH. This phenomenon hints that the reaction between •OH and H_2O_2 is one of consumption paths of H_2O_2 (reaction (10)) [44]. In case of O_2 saturated atmosphere, the signal strength decreased. Bubbling O_2 into the system will increase the concentration of HO_2•/$O_2^{\bullet -}$. Thus, the redundant HO_2•/$O_2^{\bullet -}$ would consume H_2O_2 to produce •OH (reaction (11)) [45,46]. Combining with reactions (10) and (11), the concentration of H_2O_2 in O_2 saturated atmosphere is decreased obviously and the photocatalytic reaction rate is increased.

3.3. The crucial role of •OH

The above experimental results can be summarized as thus: the main active species in the photocatalysis of $BaSb_2O_6$ are •OH and HO_2•/$O_2^{\bullet -}$. To determine which is crucial, the photocatalytic degradation of RhB is conducted in ethanol that is a well known scavenger for •OH but not for HO_2•/$O_2^{\bullet -}$ [47,48]. By UV irradiation, the generation of electrons and holes still takes place and the production of HO_2•/$O_2^{\bullet -}$ should happen normally, which is validated by Fig. 4(a). Under UV irradiation, the DMPO–HO_2•/$O_2^{\bullet -}$ ESR signal in ethanol is obvious. However, DMPO–•OH ESR signal does not emerge in the same condition. As shown in Fig. 4(b) RhB almost cannot be bleached. So, the HO_2•/$O_2^{\bullet -}$ cannot react with RhB directly and •OH should play the crucial role.

The relationship between photocatalytic activities and the concentration of •OH is investigated in the system. Fig. 5(a) and (b) shows that the difference in photocatalytic activities between M-$BaSb_2O_6$ and R-$BaSb_2O_6$ is very clear as well as the difference in the ESR signal strength of DMPO–•OH. Hydroxylation reaction of aromatic compound (TA) is also used to detect hydroxyl radicals in the system. By UV irradiation, fluorescent signals can be produced

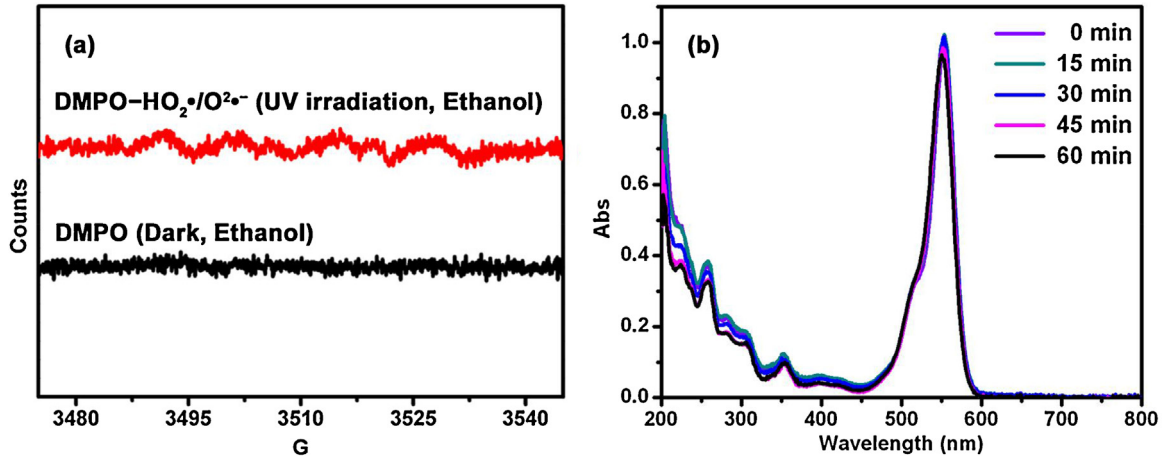

Fig. 4. The DMPO–HO_2•/$O_2^{\bullet -}$ ESR signal (a) and photocatalytic degradation of RhB over M-$BaSb_2O_6$ (b) in ethanol under UV light.

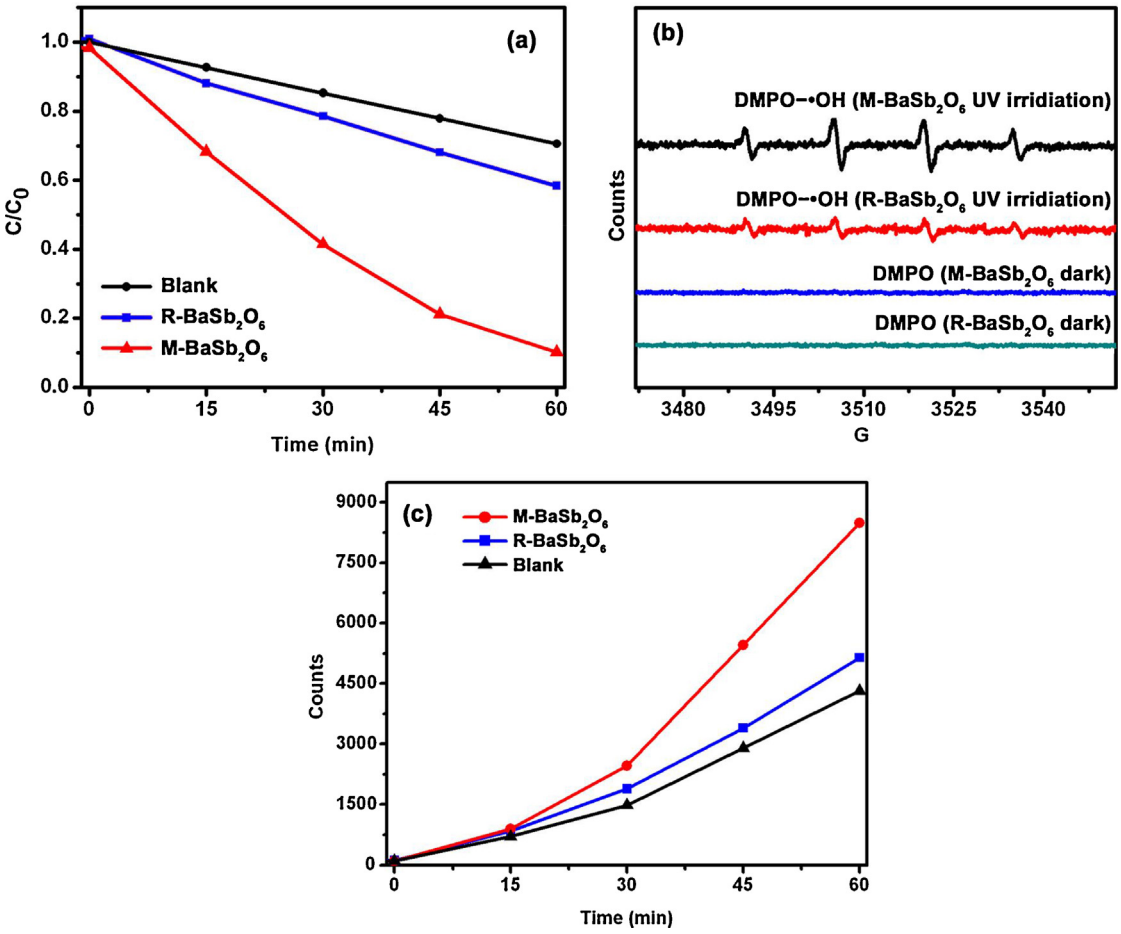

Fig. 5. The comparison of photocatalytic degradation of RhB (a), the PL-TA signal strength comparison (b) and the DMPO–•OH ESR signal strength comparison (c) between R-$BaSb_2O_6$ and M-$BaSb_2O_6$.

by adding M-$BaSb_2O_6$ or R-$BaSb_2O_6$ and the signal of M-$BaSb_2O_6$ is stronger. This phenomenon illustrates that both M-$BaSb_2O_6$ and R-$BaSb_2O_6$ can produce hydroxyl radical and M-$BaSb_2O_6$ has a better ability than R-$BaSb_2O_6$.

3.4. Morphological effect on •OH concentration

There are two main sources of hydroxyl radicals: first, the decomposition of H_2O_2; second, the oxidation of H_2O or surface hydroxyl groups by valence band holes. Then, we shall further confirm that the $HO_2^{\bullet}/O_2^{\bullet-}$, H_2O_2 and surface hydroxyl groups are closely related to the morphology of photocatalyst.

3.4.1. Morphological effect on $HO_2^{\bullet}/O_2^{\bullet-}$ and H_2O_2

As mentioned above, H_2O_2 mainly comes from $O_2 \rightarrow HO_2^{\bullet}/O_2^{\bullet-} \rightarrow H_2O_2$ (reactions (4)–(6)) and it can be decomposed to •OH through reactions (9) and (11). So, $O_2 \rightarrow HO_2^{\bullet}/O_2^{\bullet-} \rightarrow H_2O_2 \rightarrow$ •OH is a source of •OH. To further verify the rationality of this path, the formation of •OH on the surface of M-$BaSb_2O_6$ is detected by the method of PL-TA. TA reacts with •OH readily to produce a highly fluorescent product, 2-hydroxyterephthalic acid (TA-OH), whose PL peak intensity is in proportion to the amount of •OH produced in water [38]. The influences of O_2 and H_2O_2 on •OH are investigated by bubbling N_2 and the addition of catalase (an enzyme accelerating the reaction $H_2O_2 \rightarrow H_2O + O_2$) into system. As it is shown in Fig. 6, the PL signal strength of TA-OH over M-$BaSb_2O_6$ increases constantly with the prolonging time of UV illumination in air-saturated condition. When N_2 is bubbled into the reaction system to exclude DO, the PL signal is reduced observably. Interesting, the same phenomenon occurs as the catalase is added into the aerobic system. Therefore, the results of TA-OH detection further demonstrate that the reduction of •OH seems to be associated with the decrease of DO, but it essentially depends on H_2O_2 and is in accord with the results from Fig. 3.

In addition, because the reaction $O_2 \rightarrow HO_2^{\bullet}/O_2^{\bullet-} \rightarrow H_2O_2 \rightarrow$ •OH is initiated by electrons transport between photocatalyst and adsorbed oxygen, morphologies which are benefit to the oxygen adsorption and electrons transport would increase the concentration of $HO_2^{\bullet}/O_2^{\bullet-}$, H_2O_2 and ultimate •OH. To verify

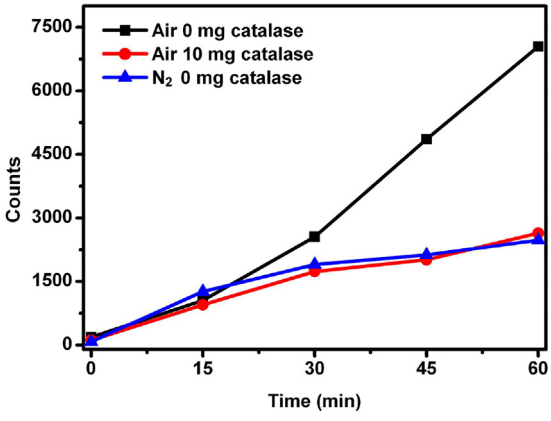

Fig. 6. PL-TA signal strength of M-$BaSb_2O_6$ in different condition.

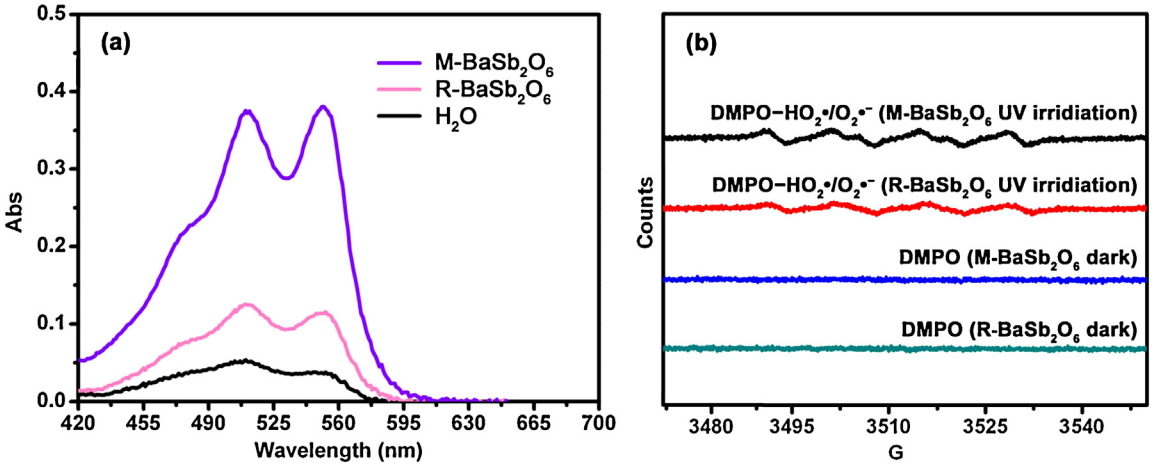

Fig. 7. Comparison of H_2O_2 signal strength (a) and the DMPO–$HO_2^{\bullet}/O_2^{\bullet-}$ ESR signal strength (b) between M-$BaSb_2O_6$ and R-$BaSb_2O_6$.

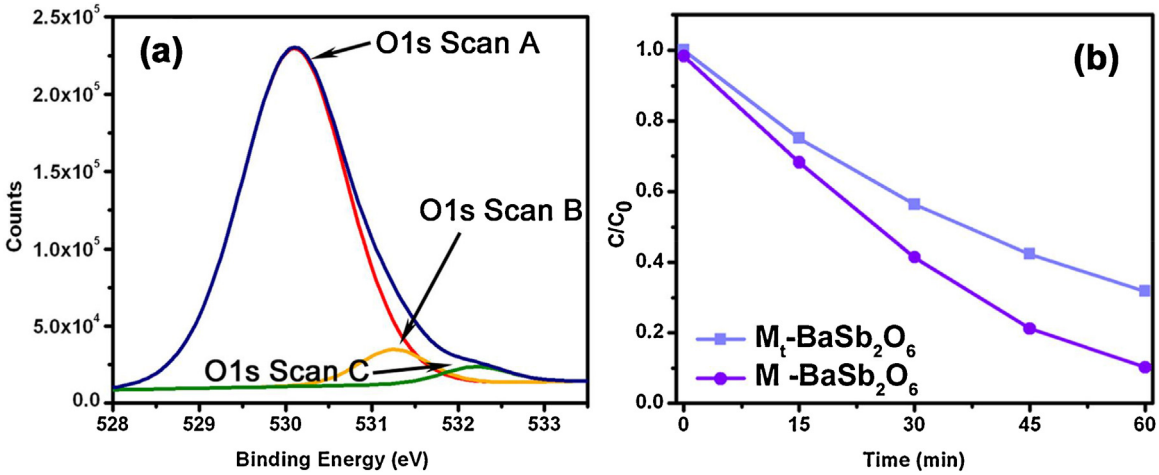

Fig. 8. O1s X-ray photoelectron spectra of M-$BaSb_2O_6$ (a) and comparison of photocatalytic activities between M-$BaSb_2O_6$ and M_t-$BaSb_2O_6$ (b).

this, the concentrations of $HO_2^{\bullet}/O_2^{\bullet-}$ and H_2O_2 are compared between M-$BaSb_2O_6$ and R-$BaSb_2O_6$. As shown in Fig. 7, stronger signals of $HO_2^{\bullet}/O_2^{\bullet-}$ and H_2O_2 can be detected over M-$BaSb_2O_6$ than that of R-$BaSb_2O_6$. It demonstrates that the production of $HO_2^{\bullet}/O_2^{\bullet-}$and H_2O_2 is indeed dependent on morphology. Therefore, M-$BaSb_2O_6$ has the favorable morphology that easily causes the reaction $O_2 \rightarrow HO_2^{\bullet}/O_2^{\bullet-} \rightarrow H_2O_2 \rightarrow {}^{\bullet}OH$ occurrence, which ultimately increases the concentration of $^{\bullet}OH$ in the system.

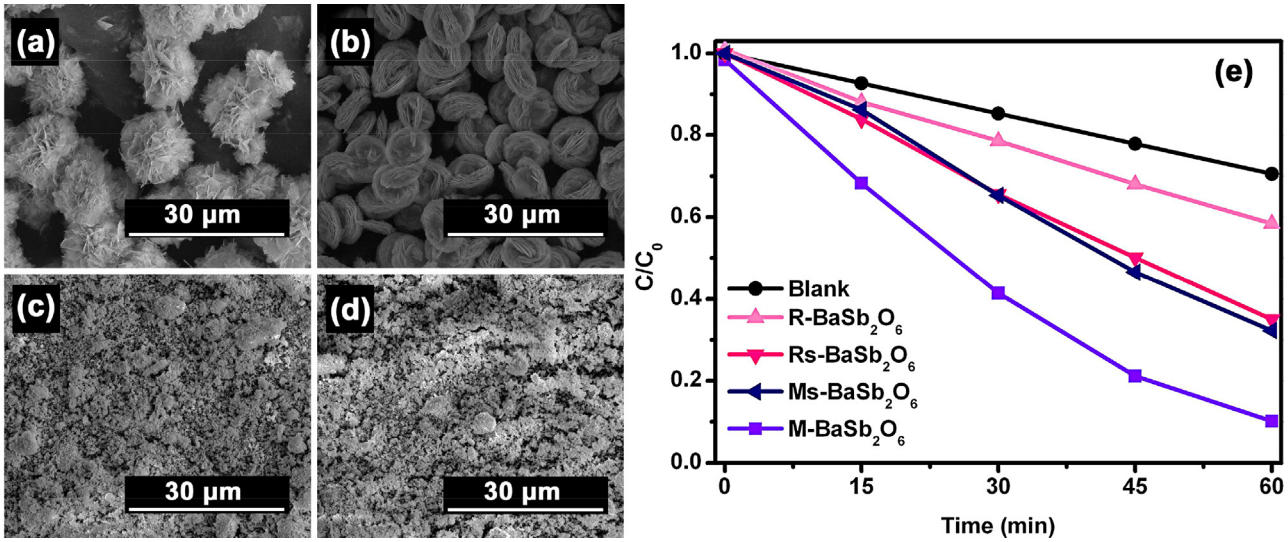

Fig. 9. The SEM of M-$BaSb_2O_6$ (a), R-$BaSb_2O_6$ (b), Ms-$BaSb_2O_6$ (c) and Rs-$BaSb_2O_6$ (d), Photocatalytic activities comparison among M-$BaSb_2O_6$, R-$BaSb_2O_6$, Ms-$BaSb_2O_6$ and Rs-$BaSb_2O_6$ (e).

3.4.2. Morphological effect on surface hydroxyl

Surface hydroxyl group is the other sources of hydroxyl radical [49]. The existence of surface hydroxyl groups is verified by XPS. Fig. 8(a) shows the O1s core level spectrum. It develops a distinct asymmetry to the high binding energy side. By curve fitting, besides the main peak of O1s located at 530.1 eV corresponding to lattice oxygen, two shoulder peaks at higher binding energy of 531.2 eV and 532.2 eV can be attributed to adsorbed oxygen and surface hydroxyl [50].

To explain the relationship between the quantity of acidic hydroxyl groups and photocatalytic activity, the acidic hydroxyl groups on the surface of M-$BaSb_2O_6$ is reduced by neutralization reaction. The mixture of M-$BaSb_2O_6$ and NaOH (2 mmol L^{-1}) is stirred for 12 h, and then the sample is collected by centrifugation and dried in 80 °C oven (the sample is denoted as M_t-$BaSb_2O_6$). Fig. 8(b) shows the photocatalytic activities of M_t-$BaSb_2O_6$ and M-$BaSb_2O_6$. The photocatalytic performance of M_t-$BaSb_2O_6$ is lower than that of M-$BaSb_2O_6$ because NaOH (2 mmol L^{-1}) consumes the acid hydroxyl groups on the surface of $BaSb_2O_6$.

The quantity of surface hydroxyl groups should be closely related to morphology. Thus, the quantities of acidic hydroxyl groups over M-$BaSb_2O_6$ or R-$BaSb_2O_6$ are measured by acid–base titration. There are 0.873 mmol g^{-1} and 0.547 mmol g^{-1} acidic hydroxyl groups on the surface of M-$BaSb_2O_6$ and R-$BaSb_2O_6$. That is, M-$BaSb_2O_6$ has more acidic hydroxyl groups than R-$BaSb_2O_6$. Then, the morphologies of M-$BaSb_2O_6$ and R-$BaSb_2O_6$ (Fig. 9(a) and (b)) are changed into irregular particles by grinding (Fig. 9(c) and (d)). The grinding samples are denoted as Ms-$BaSb_2O_6$ and Rs-$BaSb_2O_6$, respectively. The quantity of acidic hydroxyl groups over Ms-$BaSb_2O_6$ and Rs-$BaSb_2O_6$ are 0.741 mmol g^{-1} and 0.706 mmol g^{-1}, which are between those R-$BaSb_2O_6$ and M-$BaSb_2O_6$. As surface hydroxyl group is one of the sources of hydroxyl radical which plays the most important role in the $BaSb_2O_6$ photocatalysis, the photocatalytic activities of Ms-$BaSb_2O_6$ and Rs-$BaSb_2O_6$ should be higher than R-$BaSb_2O_6$ and lower than M-$BaSb_2O_6$. The photocatalytic activities presented in Fig. 9(e) confirms our guess. Therefore, changing the morphology of $BaSb_2O_6$ will influence the quantities of surface hydroxyl groups, which ultimately affects its photocatalytic performance.

4. Conclusions

The main active species and their roles in the $BaSb_2O_6$ photocatalysis are investigated. •OH plays a crucial role in the system because it strongly influences the photocatalytic activity of $BaSb_2O_6$. As the sources of •OH, the amount of $HO_2^{\bullet}/O_2^{\bullet-}$, H_2O_2 and surface hydroxyl groups are close related to the morphology, which cause the concentration of •OH is dependent on morphology. This result indicates that the potential of $BaSb_2O_6$ or other antimonates may be awaken up via modifying their morphology.

Supporting information

The morphologies, optical properties, crystallinity, surface areas and pore structures of R-$BaSb_2O_6$ and M-$BaSb_2O_6$; the consumption of DO during M-$BaSb_2O_6$ photocatalysis at N_2 saturated atmosphere; photocatalytic degradation of RhB over M-$BaSb_2O_6$ under different conditions with exposure to UV light: (a) original condition and (b) 1×10^3 mol L^{-1} EDTA.

Acknowledgments

This work was financially supported by the NNSF of China (21173047, 21373049 and 21033003), and the National Basic Research Program of China (973 Program, 2013CB632405).

Appendix A. Supplementary data

Supplementary data associated with this article can be found, in the online version, at http://dx.doi.org/10.1016/j.apcatb.2014.08.014.

References

[1] H. Xue, Z. Li, H. Dong, L. Wu, X. Wang, X. Fu, Cryst. Growth Des. 8 (2008) 4469–4475.
[2] J. Sato, N. Saito, H. Nishiyama, Y. Inoue, J. Photochem. Photobiol. A 148 (2002) 85–89.
[3] H. Mizoguchi, P.M. Woodward, Chem. Mater. 16 (2004) 5233–5248.
[4] X. Lin, F. Huang, W. Wang, Y. Wang, Y. Xia, J. Shi, Appl. Catal. A: Gen. 313 (2006) 218–223.
[5] H. Xue, Z. Li, L. Wu, Z. Ding, X. Wang, X. Fu, J. Phys. Chem. C 112 (2008) 5850–5855.
[6] J. Chen, D. Li, J. Hu, W. Chen, J. Wang, Y. Hu, X. Fu, Y. Shao, CrystEngComm 14 (2012) 8382–8389.
[7] X. Lin, J. Wu, X. Lu, Z. Shan, W. Wang, F. Huang, Phys. Chem. Chem. Phys. 11 (2009) 10047–10052.
[8] M. Sun, D.Z. Li, Y.B. Chen, W. Chen, W.J. Li, Y.H. He, X.Z. Fu, J. Phys. Chem. C 113 (2009) 13825–13831.
[9] M. Sun, D.Z. Li, Y. Zheng, W.J. Zhang, Y. Shao, Y.B. Chen, W.J. Li, X.Z. Fu, Environ. Sci. Technol. 43 (2009) 7877–7882.
[10] R. Huang, X. Xu, J. Zhu, W. Liu, R. Yuan, X. Fu, Y. Zhang, Z. Li, Appl. Catal. B: Environ. 127 (2012) 205–211.
[11] M. Sun, D. Li, W. Zhang, Z. Chen, H. Huang, W. Li, Y. He, X. Fu, J. Phys. Chem. C 113 (2009) 14916–14921.
[12] S. Jiao, G. Pang, H. Liang, Y. Chen, S. Feng, J. Nanopart. Res. 9 (2006) 605–610.
[13] Q. You, Y. Fu, Z. Ding, L. Wu, X. Wang, Z. Li, Dalton Trans. 40 (2011) 5774–5780.
[14] X. Lin, F. Huang, W. Wang, K. Zhang, Appl. Catal. A: Gen. 307 (2006) 257–262.
[15] K.-L. Zhang, X.-P. Lin, F.-Q. Huang, W.-D. Wang, J. Mol. Catal. A: Chem. 258 (2006) 185–190.
[16] W. Wang, G. Li, N. Yang, W. Zhang, Mater. Chem. Phys. 123 (2010) 322–325.
[17] T. Kako, N. Kikugawa, J. Ye, Catal. Today 131 (2008) 197–202.
[18] J. Singh, S. Uma, J. Phys. Chem. C 113 (2009) 12483–12488.
[19] T. Kako, J. Ye, J. Mol. Catal. A: Chem. 320 (2010) 79–84.
[20] W. Liu, P. Lin, H. Jin, H. Xue, Y. Zhang, Z. Li, J. Mol. Catal. A: Chem. 349 (2011) 80–85.
[21] S.J. Wu, G.Q. Li, Y. Zhang, W.F. Zhang, Mater. Res. Bull. 48 (2013) 1117–1121.
[22] J. Shi, L. Ma, P. Wu, Z. Zhou, P. Guo, S. Shen, D. Jing, L. Guo, Nano Res. 5 (2012) 576–583.
[23] J. Sato, H. Kobayashi, N. Saito, H. Nishiyama, Y. Inoue, J. Photochem. Photobiol. A 158 (2003) 139–144.
[24] J. Sato, H. Kobayashi, K. Ikarashi, N. Saito, H. Nishiyama, Y. Inoue, J. Phys. Chem. B 108 (2004) 4369–4375.
[25] J. Sato, N. Saito, H. Nishiyama, Y. Inoue, J. Phys. Chem. B 105 (2001) 6061–6063.
[26] Y. Hou, L. Wu, X. Wang, Z. Ding, Z. Li, X. Fu, J. Catal. 250 (2007) 12–18.
[27] W. Chen, H. Ruan, Y. Hu, D. Li, Z. Chen, J. Xian, J. Chen, X. Fu, Y. Shao, Y. Zheng, CrystEngComm 14 (2012) 6295.
[28] S. Meng, D. Li, X. Zheng, J. Wang, J. Chen, J. Fang, Y. Shao, X. Fu, J. Mater. Chem. A 1 (2013) 2744.
[29] L.W. Zhang, Y.J. Wang, H.Y. Cheng, W.Q. Yao, Y.F. Zhu, Adv. Mater. 21 (2009) 1286–1290.
[30] L. Chen, W. Guo, Y. Yang, A. Zhang, S. Zhang, Y. Guo, Y. Guo, Phys. Chem. Chem. Phys. 15 (2013) 8342–8351.
[31] G. Tian, Y. Chen, W. Zhou, K. Pan, C. Tian, X.-r. Huang, H. Fu, CrystEngComm 13 (2011) 2994–3000.
[32] H. Choi, E. Stathatos, D.D. Dionysiou, Appl. Catal. B 63 (2006) 60–67.
[33] W. Li, D. Li, Y. Lin, P. Wang, W. Chen, X. Fu, Y. Shao, J. Phys. Chem. C 116 (2012) 3552–3560.
[34] C. Minero, F. Catozzo, E. Pelizzetti, Langmuir 8 (1992) 481–486.
[35] H. Kita, N. Henmi, K. Shimazu, H. Hattori, K. Tanabe, J. Chem. Soc., Faraday Trans. 1: Phys. Chem. Condens. Phases 77 (1981) 2451–2463.
[36] H. Tamura, A. Tanaka, K.-y. Mita, R. Furuichi, J. Colloid Interface Sci. 209 (1999) 225–231.
[37] H.P. Boehm, Discuss. Faraday Soc. 52 (1971) 264–275.
[38] T.J. Mason, J.P. Lorimer, D.M. Bates, Y. Zhao, Ultrason. Sonochem. 1 (1994) S91–S95.
[39] K. Lv, Y. Xu, J. Phys. Chem. B 110 (2006) 6204–6212.
[40] A.H. Nethercot Jr., Phys. Rev. Lett. 33 (1974) 1088–1091.
[41] M.A. Butler, D.S. Ginley, J. Electrochem. Soc. 125 (1978) 228–232.
[42] H. Bader, V. Sturzenegger, J. Hoigné, Water Res. 22 (1988) 1109–1115.
[43] J. Yi, C. Bahrini, C. Schoemaecker, C. Fittschen, W. Choi, J. Phys. Chem. C 116 (2012) 10090–10097.
[44] D.-H. Tseng, L.-C. Juang, H.-H. Huang, Int. J. Photoenergy 2012 (2012) 1–9.
[45] T. Hirakawa, Y. Nosaka, Langmuir 18 (2002) 3247–3254.
[46] G. Vincent, A. Aluculesei, A. Parker, C. Fittschen, O. Zahraa, P.-M. Marquaire, J. Chem. Phys. C 112 (2008) 9115–9119.
[47] A. Bosnjakovic, S. Schlick, J. Phys. Chem. B 110 (2006) 10720–10728.
[48] B.H.J. Bielski, J.M. Gebicki, J. Am. Chem. Soc. 104 (1982) 796–798.
[49] P. Salvador, J. Chem. Phys. C 111 (2007) 17038–17043.
[50] G. Lu, S.L. Bernasek, J. Schwartz, Surf. Sci. 458 (2000) 80–90.